An optical fiber infrasound sensor: A new lower limit on atmospheric pressure noise between 1 and 10 Hz

Mark A. Zumberge, Jonathan Berger, Michael A. H. Hedlin, Eric Husmann, and Scott Nooner
The Cecil and Ida Green Institute of Geophysics and Planetary Physics, Scripps Institution of Oceanography, University of California—San Diego, La Jolla, California 92093-0225

Richard Hilt
Colorado College, 14 East Cache La Poudre, Colorado Springs, Colorado 80903

Rudolf Widmer-Schnidrig
Black Forest Observatory, Institute of Geophysics, Stuttgart University, Heubach 206, D-77709 Wolfach, Germany

(Received 21 June 2002; revised 17 January 2003; accepted 10 February 2003)

A new distributed sensor for detecting pressure variations caused by distant sources has been developed. The instrument reduces noise due to air turbulence in the infrasound band by averaging pressure along a line by means of monitoring strain in a long tubular diaphragm with an optical fiber interferometer. Above 1 Hz, the optical fiber infrasound sensor (OFIS) is less noisy than sensors relying on mechanical filters. Records collected from an 89-m-long OFIS indicate a new low noise limit in the band from 1 to 10 Hz. Because the OFIS integrates pressure variations at light-speed rather than the speed of sound, phase delays of the acoustical signals caused by the sensor are negligible. Very long fiber-optic sensors are feasible and hold the promise of better wind-noise reduction than can be achieved with acoustical-mechanical systems. © *2003 Acoustical Society of America.* [DOI: 10.1121/1.1566978]

PACS numbers: 43.28.Dm, 43.38.Hz [LCS]

I. INTRODUCTION

Atmospheric pressure changes that occur faster than those due to weather and slower than can be sensed by human hearing, termed infrasound, are caused by many natural and anthropogenic sources. Bolides, lightning, earthquakes, volcanoes, and ocean waves are examples of the former; supersonic aircraft and explosions are included in the latter. The Comprehensive Test Ban Treaty (CTBT) for nuclear weapons has fostered a renewed interest in infrasound in the band from 0.01 to 10 Hz. A worldwide network of 60 infrasound stations is being established to help monitor compliance with the treaty (Christie *et al.*, 2001).

Wind turbulence is a major source of noise in the infrasonic band. Hedlin *et al.* (2002), for example, reported that the noise power between 0.1 and 1 Hz in a moderately filtered microbarometer rose about 20 dB as the wind speed increased from 1 to 5 m/s. To combat this problem, researchers have developed a number of acoustical-mechanical spatial filters consisting of multiple inlet ports connected via pipes to a microbarometer in hopes of averaging out wind noise (e.g., Daniels, 1959; Burridge, 1971; Alcoverro and LePichon, 2002; Hedlin *et al.*, in press). These have proven somewhat successful, but higher frequency sampling of the pressure field is limited by time delays in these mechanical filters. An alternative would be to deploy several hundred individual sensors and data recorders over a large area, but that is not very practical.

We report here on another alternative. We have constructed a distributed pressure sensor, which averages pressure along a line by means of fiber optic sensing of strain in a long tubular diaphragm. The sensitivity to pressure changes has proven to be superior to other techniques in the band from 1 to 10 Hz. The sensor provides a continuous signal representing the instantaneous spatial average of pressure along the line described by the sensor. This average pressure $\overline{P}(t)$ at time t along path S is given by

$$\overline{P}(t)=\left(\frac{1}{L}\right)\oint_S P(s,t)ds. \tag{1}$$

In principle, the length L of path S can be made up to several km if desired.

Our original design consisted of an unconstrained optical fiber, exposed to ambient pressure, monitored with a laser interferometer. Such a design takes advantage of the fact that an optical fiber responds inherently to pressure changes via its strain-optic effect (Hocker, 1979). We formed an interferometer consisting of two optical fibers placed side-by-side (to make temperature effects common-mode) with one of them (the reference fiber) encased inside a stiff, sealed tube to shield it from pressure fluctuations. Early experiments revealed, however, that strains in the loose fibers caused noise larger than the small pressure signals we hoped to detect. This led us to the compliant tube as a means of increasing the pressure-induced strain in the fiber. This is described below.

II. DESCRIPTION OF THE INSTRUMENT

We call our new sensor, shown in Fig. 1, an optical fiber infrasound sensor (OFIS). We use a compliant, sealed tube

 0001-4966/2003/113(5)/2474/6/$19.00

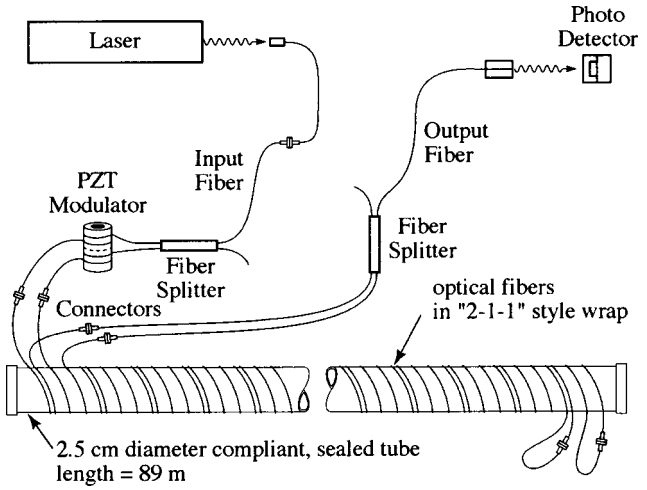

FIG. 1. The OFIS (optical fiber infrasound sensor) consists of a sealed compliant tube wrapped with a pair of optical fibers. The fibers respond to mechanical strain in the tube caused by ambient pressure changes. The "2-1-1" wrap results in one of the two fibers being strained more than the other under pressure changes. The path length difference is monitored interferometrically.

(25-mm-diam silicon rubber with 3-mm wall thickness) helically wrapped with optical fiber (SMF28 single mode with 900-μm buffer). As the ambient pressure around the tube changes, its diameter changes in response and strains the optical fiber; this strain is monitored interferometrically. This technique is sensitive to the integrated pressure along the tube, and we can build the tube almost arbitrarily long. Because the apparent pressure change inferred from the observed optical path change along a fiber wrapped around a tube of length L is governed by Eq. (1), the pressure variations having a spatial scale shorter than the total length of the sensor will be averaged away. The sensor is a true, linear, integrator whose incremental step-size is the order of the tube diameter (25 mm). Because the phase delay variation along the fiber is governed by the speed of light rather than the speed of sound as in the acoustical-mechanical filters, the response is flat up to relatively high frequencies (initial tests indicate attenuation begins around 2 kHz). The issue of how the deployment geometry [path S in Eq. (1)] affects the response is addressed in Sec. IV.

We built a wrapping machine to construct the fiber-wrapped tube depicted in Fig. 1. The compliant tubing is fed into one end of the machine at a constant rate while spools of optical fiber orbit around the tube, leaving behind helical wraps. Small electric motors control the tension on each fiber spool to maintain uniformity; similarly the feed rate of the tube and the rotation rate of the fiber spools is controlled to yield a constant spacing between the wraps. The machine also wraps a layer of silicon ribbon over the fibers to keep them in place. The interval between repeat fiber wraps is 55 mm.

To obtain immunity from slight wavelength fluctuations in the laser which illuminates the interferometer (a distributed feedback laser diode with wavelength $\lambda_1 = 1310\,\text{nm}$), we use an equal-arm Mach-Zender interferometer (Hocker, 1979). In such a device, the difference in the optical path lengths of two identical optical fibers is sensed. We optimize the sensor by configuring the mechanical coupling between the optical fibers and the compliant tube such that the signal of interest affects one fiber more than the other while sources of noise have the same effect on both fibers (i.e., common mode rejection). For example, the fibers themselves have temperature coefficients, but to a good approximation, both experience the same temperature environment, and—being differential—the interferometer is unaffected. By spacing the wraps of the two fibers as shown in Fig. 1, one fiber experiences approximately twice the strain as the other as the tube deforms from pressure changes. The fibers wound closely together strengthen one another and hence strain less (for a given pressure difference) than the two isolated fibers.

The interferometer must track both increases and decreases in the optical path length difference. In order to do this, we form two fringe signals: the first is the direct signal (V_x), which is output of the photodetector in Fig. 1, the second (V_y) is generated in quadrature with the first. This is achieved with a lock-in amplifier while modulating the length difference by a small fraction of a wavelength at several hundred kHz by means of a piezoelectric crystal. The lock-in amplifier's phase is adjusted to produce the derivative of the direct fringe signal. When plotted against each other, V_x and V_y trace out an ellipse as the optical path changes. The instantaneous position on the ellipse perimeter is a measure of the optical path length difference. We recorded the two voltages V_x and V_y at 200 samples per second in the work reported here. Then we processed the records in 15-min segments by fitting the samples to an ellipse given by the parametric equations $V_x = A\sin(\phi+\delta)$ and $V_y = B\cos(\phi)$, where A and B are the amplitudes of the two fringe signals, δ is related to the eccentricity of the ellipse, and ϕ is the desired optical phase difference related to the optical path length change $dL_{\text{opt}} = (\lambda_1/2\pi)\phi$. (We analyzed 15-min-long data segments because slowly varying perturbations to the polarization and the laser output power produce drift in the ellipse coefficients.) The spatially integrated, instantaneous, relative pressure $P(t)$ is given by $P(t) = (\alpha/L)\phi(t)$, where α is the empirically determined sensitivity, governed by the rheological coefficients of the rubber tube, the fibers, and the tension and spacing of the fibers. Laboratory and field experiments have determined that α is 2.52 Pa m rad^{-1}. The time series of $\phi(t)$, extracted from the records of $V_x(t)$ and $V_y(t)$, gives the record of pressure fluctuations averaged along the sensor length.

We deployed a sensor having $L = 89\,\text{m}$ at our geophysical test facility, Piñon Flat Observatory, in the high desert south of Palm Springs, CA (see Fig. 2 for the location). In this deployment, we buried the sensor beneath a shallow layer of gravel to protect it from wildlife and rapidly varying thermal effects. As shown in Fig. 3, the sensor itself was below the surface by a distance of about 20 cm, covered by sorted gravel with typical rock diameter of 9 mm. Experiments in our lab showed that the acoustic attenuation produced by the gravel is insignificant at frequencies below 20 Hz. The fringe signal was continuously sampled at 200 samples per second with a 24-bit digitizer (18 bits are required to resolve 1 μPa). The data were telemetered to our

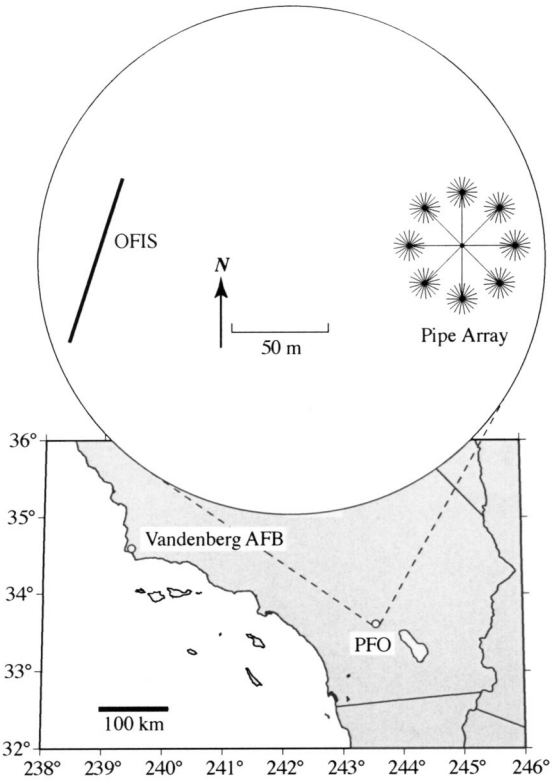

FIG. 2. Our first field test of the OFIS occurred at Piñon Flat Observatory (PFO) in the high desert just south of Palm Springs, CA. We oriented the sensor such that wave fronts from sources at Vandenberg Air Force Base would arrive parallel to the sensor. Several pipe array infrasonic sensors are also sited at PFO.

lab where the fringe signal postprocessing was performed to extract the pressure records.

After installation, we calibrated the sensor by imposing a small pressure difference (measured with a Paroscientific quartz gauge) by pumping air into the sensor tube and recording the fringe signal. A 30-cm-long capillary tube (having 0.25-mm inside diameter) connected the inside of the tube to the ambient atmosphere so that slowly changing pressure (with a time constant longer than 10 mins) would not be detected.

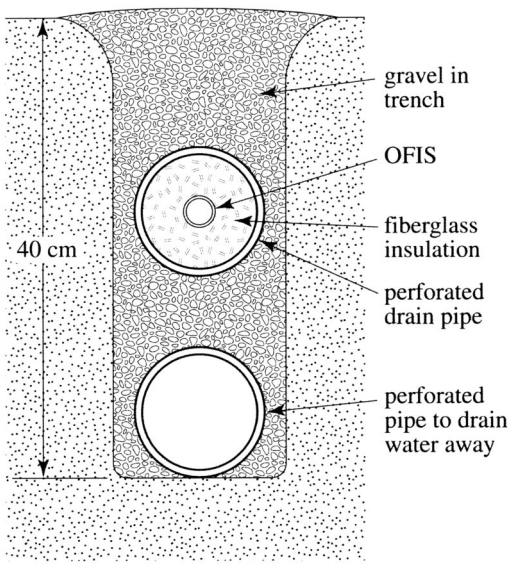

FIG. 3. This is a vertical cross section of the OFIS as it is deployed in a trench at the field site.

We have compared recordings from the new fiber-optic sensor with time series collected simultaneously from two other sensors approximately 150 m away (see the map in Fig. 2). The other sensors, described in detail elsewhere (Hedlin *et al.*, 2002), consist of two types of acoustical-mechanical filters covering a circular region 70 m in diameter connected to two microbarometers. One of the arrays, which we refer to as the Pipe Array, follows the design established for the CTBT (Christie *et al.*, 2001). A microbarometer in the center of the Pipe Array is connected to eight 27-m-long pipes extending radially in a symmetric pattern. Each of these pipes is connected to a manifold joining 18 8-m-long pipes (each open at its end) splayed into secondary symmetric patterns (see Fig. 2). This plumbing results in 144 ports each connected to the microbarometer via 35 m of solid pipe.

The Hose Array consists of eight 16-m-diam rings of compliant, microporous hose colocated with the Pipe Array ports; a point on the inner edge of each hose ring is connected to the array's microbarometer via a 19-m-long solid pipe. Spatially, the Hose Array samples essentially the same pattern as the Pipe Array, but the acoustic path lengths between points on the hose ring and the microbarometer vary from 19 to 69 m.

III. RESULTS

An example of a pressure event recorded with these sensors is displayed in Fig. 4. This is the signal produced by the launch of an Atlas II rocket from Vandenberg Air Force Base (AFB) 396 km away on 8 September 2001. Note that we purposely oriented the OFIS along an azimuth normal to the direction to Vandenberg AFB so that wave fronts from signals generated there would arrive parallel to our linear sensor (Fig. 2). The signal to noise in the OFIS record compares favorably with the other sensors operating at the same time (the records displayed in Fig. 4 have been band-pass filtered from 0.5 to 10 Hz). The Pipe Array displays the noise that results from internal resonances that have been reported elsewhere (Alcoverro and LePichon, 2002; Hedlin *et al.*, 2002). These resonances have subsequently been attenuated using strategically placed orifices in the pipe arrays deployed in support of the CTBT rendering their responses to be essentially like that of the Hose Array shown here.

Figure 5 shows the transfer function (or relative response) of the OFIS and the Hose Array computed from the time series in Fig. 4; we have plotted the ratio of the Hose Array response divided by the OFIS response. Because the Hose Array was sampled at 20 samples per second and low-pass filtered with a 9-Hz cutoff, we limit our analysis to frequencies below 10 Hz, even though the OFIS is responsive to at least 100 Hz. Note that the independent calibrations of the two sensors appear to corroborate one another: the relative response is near unity between 0.2 Hz and about 3 Hz. Because the relative response drops above 3 Hz, either the response of the Hose Array decreases there or the response of the OFIS increases. We have good evidence that it

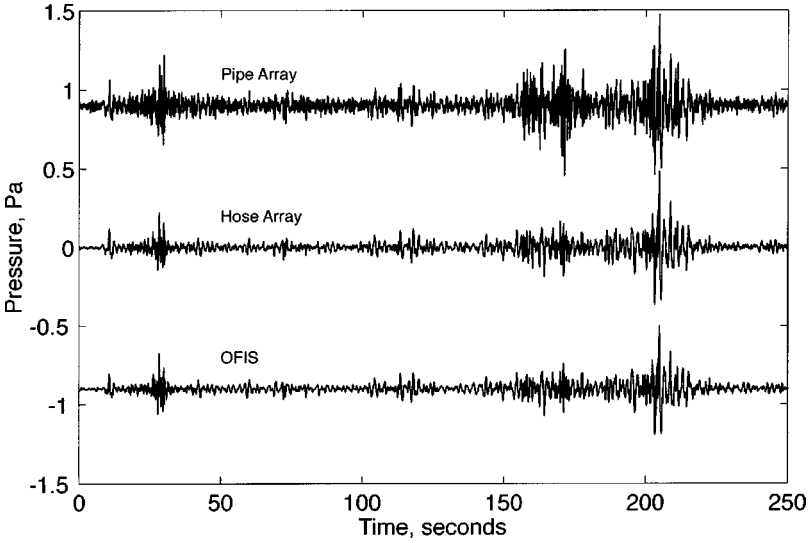

FIG. 4. These are time series of pressure variations recorded by three sensors at PFO. The source is an Atlas II rocket launch at Vandenberg AFB.

is the decrease in response of the Hose Array caused by its finite size and deployment shape that is responsible for the decrease above 3 Hz (see below).

Pressure noise increases with wind speed. To investigate the importance of wind on this sensor's performance, we computed power spectra for 440 contiguous 15-min intervals over a 4-day period for all three of the sensors described here. Two examples are shown in Fig. 6. One [Fig. 6(a)] was recorded during an interval where the average wind speed was 1.4 m/s, the other [Fig. 6(b)] at 3.3 m/s. In the low wind case, the microbarom peak at 0.2 Hz is clearly evident. It becomes obscured by ambient noise at higher wind speeds. (The wind speed during the time of the data shown in Fig. 4 was 1.8 m/s.)

Wind noise may affect the sensors slightly differently (and they are not exactly co-located). We therefore computed the minimum noise per band for all three sensors to determine the noise floor for each. After computing the 440 spectra for each sensor, we found the minimum power level in each frequency bin for each sensor. These minimum spectra are shown in Fig. 7. Each point represents the lowest 15-min-averaged power observed over the 4-day period for a specific frequency—the collection of points in these curves were not necessarily gathered in the same 15-min intervals or under the same wind speeds, they are simply the 4-day power minima irrespective of all else. Several aspects of these spectra are worth noting. First, the microbarom peak is evident in each. Second, the OFIS is slightly noisier at frequencies below 0.2 Hz. We suspect residual thermal noise is responsible. The most significant difference is that the OFIS's minimum noise per band is significantly lower than that of the others above 1 Hz; the improvement is about 23 dB at 8 Hz. We know that this represents a real improvement in the sensing methodology rather than a result of a roll-off in the frequency response of the OFIS because we examined the relative responses of the OFIS and the Hose Array (Fig.

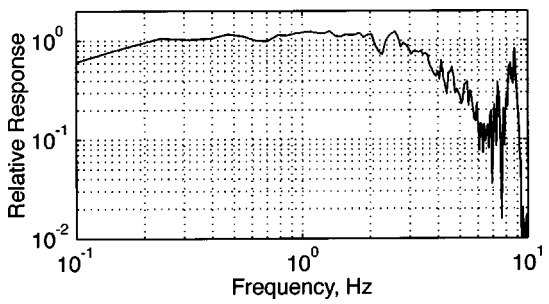

FIG. 5. The transfer function (Hose Array response divided by the OFIS response) was computed from the time series shown in Fig. 4.

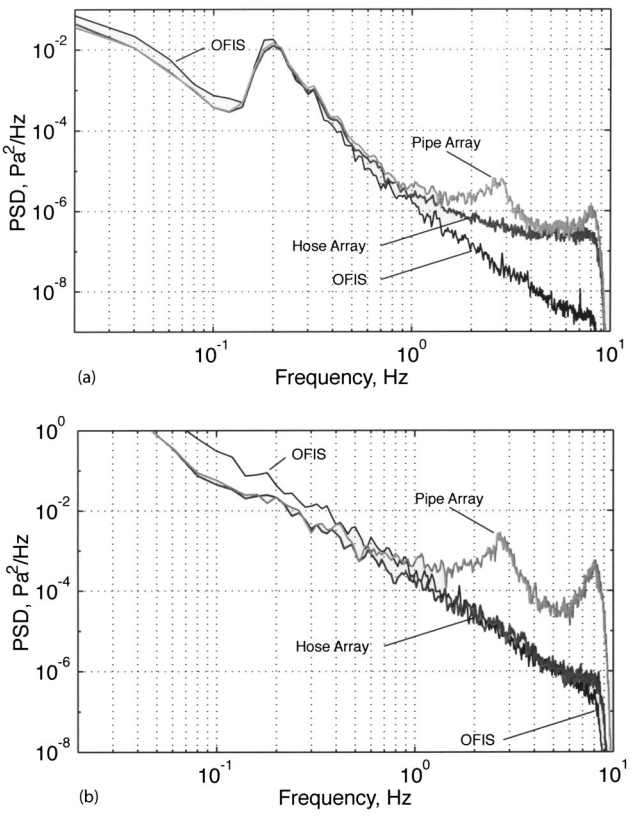

FIG. 6. (a) Power spectral densities from three sensors recorded simultaneously during a 15-min-long period when the wind speed averaged 1.4 m/s. The peak at 0.2 Hz is from the microbarom background. The peaks in the Pipe Array at 3 and 8 Hz are from internal resonances. (b) Same as (a) except the average wind speed was 3.4 m/s.

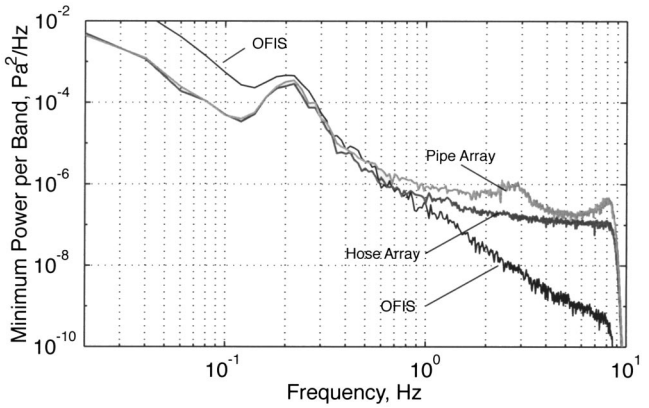

FIG. 7. Spectra were computed for each sensor for 440 15-min-long contiguous time segments. The minimum power level for each band is plotted.

5). We have seen that the response of the OFIS is flat to at least 3 Hz and is likely flat to about 1 kHz. For this case of an averaging dimension of the order of 100 m, we believe that the noise floor in Fig. 7 for the OFIS represents a new lower limit on spatially averaged ambient atmospheric pressure noise in the band from 1 to 10 Hz.

It may be that the results from the hose and pipe arrays are limited by the noise of their microbarometers (MB2000 DASE Tekelec). It has been reported that the Chaparral 4.11 sensors have lower noise (Kromer *et al.*, 1998). Standard infrasound microphones (B&K Model 4193 with preamplifier 2193, for example) have instrument noise as reported by the manufacturer's literature (Bruel & Kjaer Microphone Handbook, Vol. 1, part no. BE1447-11) some 3 to 12 dB higher than the noise levels measured by the OFIS in the frequency band 1 to 10 Hz.

IV. GEOMETRIC EFFECTS ON THE RESPONSE

As noted above, the OFIS was oriented to maximize its response to signals arriving from the direction of Vandenberg AFB. Being a line receiver, its response is directional. Pressure wave fronts add in phase along the entire length of the OFIS for wave vectors perpendicular to it. A line sensor will average over several cycles of the wave-train for arrivals from other directions if the wavelength λ_P is smaller than the sensor length L.

A pressure wave traveling in the x direction (Fig. 8) with amplitude P_0, wave number $k=2\pi/\lambda_P$, and angular frequency ω is described by

$$P(x,t)=P_0\sin(kx-\omega t). \tag{2}$$

Substituting this into Eq. (1) gives the spatial average of this wave field at time t along a straight path of length L aligned at an angle θ relative to the x direction:

$$\overline{P}(t)=\frac{1}{L}\int_0^L P_0\sin(kl\cos\theta-\omega t)\,dl \tag{3}$$

(l is the position along the averaging path). Evaluation of this integral yields the ratio R of the amplitude of the line-averaged pressure signal to the amplitude of the traveling pressure signal:

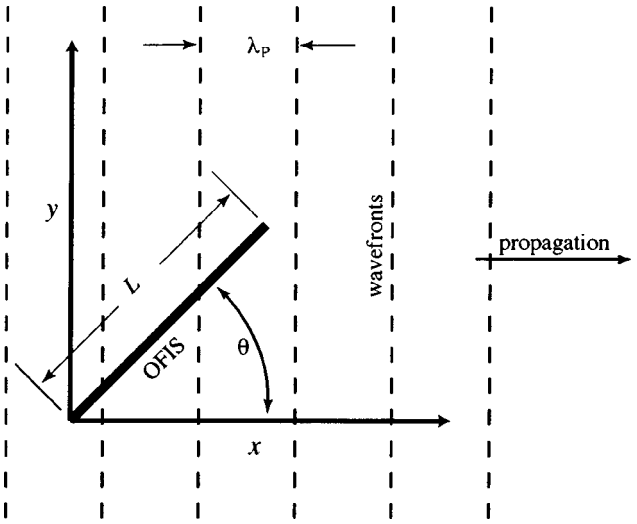

FIG. 8. The geometry for Eqs. (2)–(4).

$$R(\theta)=\frac{\sin(N\pi\cos\theta)}{N\pi\cos\theta}, \tag{4}$$

where $N=L/\lambda_P$. Figure 9 displays R vs. θ for $N=2.6$ (the solid curve) and $N=0.26$ (the dashed curve), corresponding to plane waves traveling at 340 m s^{-1} horizontally across the sensor having frequencies of 10 and 1 Hz, respectively.

Clearly, there is a frequency roll-off for a line sensor receiving distant signals from other than $\theta=90°$. An array of several line sensors oriented along differing azimuths would be required to detect high-frequency signals from all directions. While the response of a circular sensor is omnidirectional, it begins to fall off when the wavelength approaches the sensor diameter. This can be computed numerically for any shaped sensor by summing the phasor vectors for all segments of the sensor. The phase shift at each segment having position x (again for a wave traveling in the x direction) is kx. The sensor's total response R for M segments is given by the magnitude of the vector sum of the phasors from each segment:

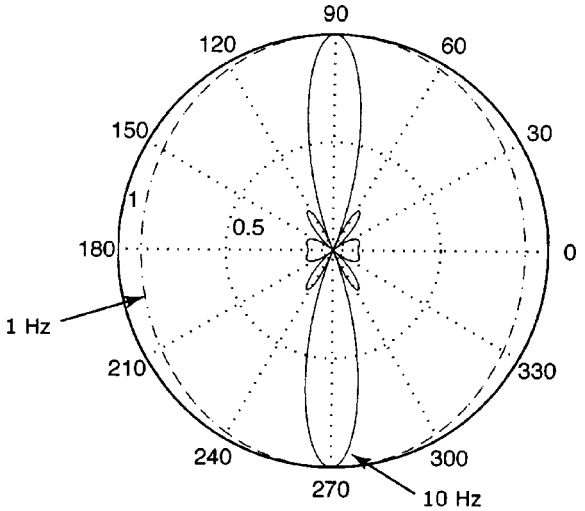

FIG. 9. The directional response of an 89-m-long OFIS is plotted for $L/\lambda_P=2.6$ (solid curve) and $L/\lambda_P=0.26$ (dashed curve).

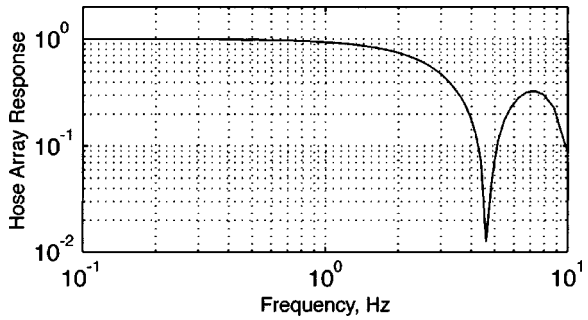

FIG. 10. The results of a numerically integrated spatial average as a function of frequency for a hose or pipe array of the geometry depicted in Fig. 2. Compare this with the observed response shown in Fig. 5.

$$R=\frac{1}{M}\left\{\left(\sum_{i=1}^{M}\cos(kx_i)\right)^2+\left(\sum_{i=1}^{M}\sin(kx_i)\right)^2\right\}^{1/2}, \qquad (5)$$

where the shape of the sensor is described by M segments each at coordinate x_i, y_i (the individual phase shifts do not depend on the y_i's because the wavefronts are assumed to be parallel to the y axis in this calculation).

This sum was computed for the geometry of the Hose Array described earlier (which is nearly the same as the geometry of the Pipe Array). Figure 10 shows the result of this numerical computation. Note that the shape of the curve in Fig. 10 agrees qualitatively with the observed transfer function between the OFIS and the Hose Array in Fig. 5. They differ somewhat in the location of the first response null (when the wavelength of the incident ray is about the same as the diameter of the Pipe Array). It is likely that other propagation effects (such as those described by Burridge, 1971) further modify the responses of the pipe arrays (it is also possible that the incident wave shown in Fig. 4 and analyzed for the comparison in Fig. 5 was not propagating horizontally). Note that this response null is purely a geometric effect resulting from our comparing a linearly deployed sensor (the OFIS) to circularly deployed sensors (the Pipe and Hose arrays) and that it will occur only for coherent waves—consequently the response null is absent from the spectra in Figs. 6 and 7 because they are dominated by ambient incoherent noise.

V. CONCLUSIONS

We have developed a new sensor for the detection of pressure variations in the infrasound band. It is less noisy than other sensors above 1 Hz, and somewhat noisier below the microbarom peak. We believe residual thermal effects in the compliant silicon tube cause this. The records we have collected reveal (as far as we are aware) a new low noise limit in the band from 1 to 10 Hz.

The prototype sensor we have built and studied is 89 m long. At this length, it reduces wind noise as well as similarly sized mechanical arrays. It would be difficult to make larger mechanical filters because the phase delays within them become more problematic as the size of the filter grows. With the OFIS, however, significantly longer lengths are possible without such problems, promising better wind noise reduction.

The directional characteristic of the linear sensor suggests that an array of them, oriented at different angles, will allow computation of direction to the source. The array arms could be made very long to reduce wind noise.

ACKNOWLEDGMENTS

Gene Herrin, Paul Golden, and Mike Sorrells provided useful insight on the effects of burying the instrument and contributed the Hose Array concept, which proved important for comparisons. This research was funded by the Defense Threat Reduction Agency under Contracts Nos. DSWA01-99-C-0056 and DTRA01-00-C-0085.

Alcoverro, B., and Le Pichon, A. (**2002**). ''Design and optimization of a noise reduction system for infrasound measurements using elements with low acoustic impedance,'' J. Acoust. Soc. Am.

Burridge, R. (**1971**). ''The acoustics of pipe arrays,'' Geophys. J. R. Astron. Soc. **26**, 53–70.

Christie, D. R., Vivas Veloso, J. A., Campus, P., Bell, M., Hoffmann, T., Langlois, A., Martysevich, P., Demirovich, E., and Carvalho, J. (**2001**). ''Detection of atmospheric nuclear explosions: the infrasound component of the International Monitoring System,'' Kerntechnik **66**, 96–101.

Daniels, F. B. (**1959**). ''Noise reducing line microphones for frequencies below 1 c/s,'' J. Acoust. Soc. Am. **31**, 529.

Hedlin, M. A. H., Alcoverro, B., and D'Spain, G. (in press). ''Evaluation of rosette infrasonic noise-reducing spatial filters,'' J. Acoust. Soc. Am.

Hedlin, M. A. H., Berger, J., and Vernon, F. L. (**2002**). ''Surveying infrasonic noise on oceanic islands,'' Pure Appl. Geophys. **159**, 1127–1152.

Hocker, G. B. (**1979**). ''Fiber-optic sensing of pressure and temperature,'' Appl. Opt. **18**, 1445–1448.

Kromer, R. P., and McDonald, T. S. (**1998**). ''Test and Evaluation of the Chaparral Physics Model 4.11 Infrasound Sensor for CTBT Infrasound Array application,'' in Proc. Infrasound Workshop for CTBT Monitoring, Santa Fe, New Mexico, 25–28 August 1997, Los Alamos National Laboratory, LA-UR-98-56.